

Nuclear structure effects on the absorption in the scattering of heavy ions at low energy

J. C. Pacheco,¹ M. D. Kadi-Hanifi,² B. Bilwes,³ and F. Remiro⁴

¹*Departamento de Física Aplicada e Instituto de Física Corpuscular, Centro Mixto CSIC Universitat de Valencia, 46100 Burjassot, Valencia, Spain*

²*Institut des Sciences Exactes, Département de Physique, Université de Blida, Blida, Algeria*

³*Institut de Recherches Subatomiques, IReS-IN2P3 BP28, 67037 Strasbourg Cedex 2, France*

⁴*Instituto Enseñanza Secundaria, Berenguer Dalmau, Catarrojo, Valencia, Spain*

(Received 22 June 1998)

Elastic scattering data for different systems, at energies close to the Coulomb barrier, are systematically analyzed with a renormalized M3Y double folding real potential and a Woods-Saxon imaginary one. Then the contribution to the imaginary potential of couplings to the low lying inelastic channels is calculated in the Feshbach formalism and shown to give too weak absorption except for strongly deformed systems, $^{35,37}\text{Cl}+^{24}\text{Mg}$. For the others systems the transfer cross sections are known to be large which implies that the coupling to transfer channels should contribute to absorption. To simulate their effect a fitted surface term is added to the Feshbach term. The radial distribution of the reaction cross section shows a strong sensitivity to the absorption but at large distances only. [S0556-2813(99)06802-8]

PACS number(s): 25.70.Bc, 24.10.-i

I. INTRODUCTION

From many years ago one knows that at low energy inelastic and transfer channels couplings give large contribution to the imaginary potential of elastic scattering at large distances. The contribution of inelastic and single-particle transfer channels has been calculated in a semiclassical approach [1,2]. Starting from the Feshbach theory of the optical potential [3] a number of attempts were performed to evaluate the nucleus-nucleus potential. In this formalism the contribution of the low lying inelastic channels is described by using microscopic [4] or macroscopic [5] form factors. The nonelastic channels were introduced either individually [4,5,6] or globally by using closure relation [7]. This last model was able to reproduce successfully the elastic scattering data [8], as well as to predict the excitation function of the near- and sub-barrier fusion for spherical or weakly deformed systems [9]. However, when the energy of the collision is close to the Coulomb barrier and the absorption is mainly due to a reduced number of inelastic channels, as it was observed in deformed systems [10], the model overestimates the absorption and it is more accurate to evaluate the polarization potential corresponding to each of the few channels that control the absorption. Nevertheless for some systems this contribution to the absorption is too weak and transfer channels become important.

Recently semiphenomenological and microscopic analyses of $^{32}\text{S}+^{24}\text{Mg}$ elastic scattering data has been successfully compared at low energy [11]. Experiments show that at low energy the 2_1^+ deformed states of $^{24}\text{Mg}(E^*=1.37\text{ MeV})$ and $^{32}\text{S}(E^*=2.23\text{ MeV})$ are the only states strongly populated. A good agreement between semiphenomenological and microscopic calculations was obtained on elastic scattering, radial absorption, and spin distributions as well as on total reaction cross section. Our analysis has shown that the total absorption is sensitive in a narrow domain of the nucleus-nucleus surface potential and that the volume absorption gives a negligible contribution to the reaction cross section.

With only a reduced number of low lying collective states it was possible to reproduce the total absorption. Motivated by the success of our calculations in reproducing the most characteristic experimental features in the case of a strongly deformed system as $^{32}\text{S}+^{24}\text{Mg}$, we have investigated if a similar behavior is observed in other deformed or spherical systems. In the present paper, we analyze a number of different systems in which the transfer processes give contributions whose importance can be similar to those due to the inelastic channels contribution. We have analyzed the experimental data for $^{32}\text{S}+^{32}\text{S}$ [12], $^{32}\text{S}+^{36}\text{S}$ [13], $^{32}\text{S}+^{28}\text{Si}$ [14], $^{32}\text{S}+^{40}\text{Ca}$ [15] systems at 90.0 MeV, as well as $^{35}\text{Cl}+^{24}\text{Mg}$ [10] at 85.0 MeV, $^{37}\text{Cl}+^{24}\text{Mg}$ [10] at 87.9 MeV, $^{31}\text{P}+^{27}\text{Al}$ [13] at 79.5 MeV, and $^{16}\text{O}+^{208}\text{Pb}$ [16] at 87.0 MeV. In all cases, the energies are just above the Coulomb barrier.

Section II describes an analysis of elastic scattering data with a renormalized double folding real potential and a phenomenological imaginary one. In Sec. III we briefly report a calculation of the contribution of the strongly excited states of target and projectile to the absorptive part of the potential using Feshbach theory and show that, for some of our systems, this contribution is not enough and it is necessary to add a phenomenological surface term to the absorptive potential fitted on elastic scattering data. The radial and spin distributions of reaction cross section are calculated in Sec. IV for both potentials of Secs. II and III. Our conclusions are proposed in Sec. V.

II. SEMIPHENOMENOLOGICAL DATA ANALYSIS

The real part of the optical potential is calculated using the double folding model [17] with an effective M3Y two-body force [18] which must be renormalized. The nuclear densities are obtained by unfolding the finite-sized charge distribution of the nucleons from the charge densities in the standard way [17]. The nuclear charge distributions included

TABLE I. Experimental charge densities $\rho_c(r) = \rho_0(1 + \omega r^2/c^2)[1 + \exp((r-c)/z)]^{-n}$.

Nucleus	c (fm)	z (fm)	ω	n	Note	Ref.
^{16}O	2.608	0.513	-0.051	1.00		[19]
^{27}Al	3.079	0.519	0.0	1.00		[19]
^{28}Si	3.239	0.574	-0.149	1.00		[20]
^{31}P	3.369	0.582	-0.173	1.00		[19]
^{32}S	3.441	0.624	-0.213	1.00		[21]
^{35}Cl	3.490	0.602	-0.120	1.00		[22]
^{37}Cl	3.554	0.588	-0.130	1.00		[19]
^{40}Ca	3.676	0.585	-0.102	1.00		[23]
^{208}Pb	7.194	0.658	0.0	1.56	neutron	[24]
^{208}Pb	6.975	0.635	0.0	1.42	proton	[24]

in Table I and Table II are taken from electron scattering experiments, except for ^{208}Pb where we use the density calculated by Brack [24] in a variational semiclassical method. For all the nuclei included in Table I the densities are parametrized in a four-parameter Fermi parabolic form while we give in Table II the coefficients of a Bessel-Fourier parametrization for the case of ^{36}S . The imaginary potential is parametrized assuming a Woods-Saxon radial form factor [25]. Our total potential is then

$$V_T(R) = N \cdot V_{M3Y}(R) + iW_{WS}(R) + V_C(R) = U(R) + iW_{WS}(R) + V_C(R), \quad (1)$$

where $V_{M3Y}(R)$ is the bare double folding real potential and N is the usual renormalization factor, $V_C(R)$ is the Coulomb potential, and $W_{WS}(R)$ is a Woods-Saxon potential. The parameters of $W_{WS}(R)$ and the renormalization factor, N , are fitted on elastic scattering data using the ECIS94 code [26]. As it is well known, at low energies the cross sections are not sensitive to the interior of the potential and to reduce the number of parameters we have fixed the imaginary potential depth to $W_0 = 60 \text{ MeV}$. The best fits (full lines) of elastic scattering data are shown in Figs. 1(a)–4(a) and correspond to the parameters of Table III, where calculated total reaction cross sections are also included.

III. POLARIZATION IMAGINARY POTENTIAL

In this section we assume that the real potential $U(R)$ is the potential of Sec. II and we propose an analysis of the imaginary potential in terms of coupling to nonelastic channels. We calculate first the contribution of inelastic channels by using the Feshbach theory and then we add a phenomenological absorptive term to simulate the transfer processes contribution.

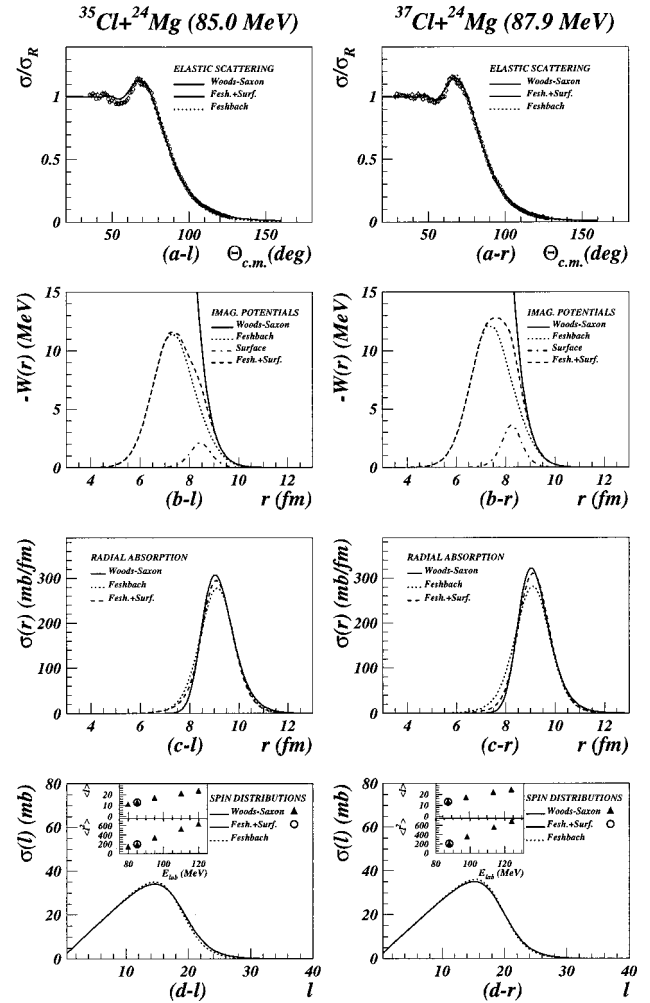


FIG. 1. Experimental data and calculations for $^{35}\text{Cl}+^{24}\text{Mg}$ system at 85.0 MeV (left) and $^{37}\text{Cl}+^{24}\text{Mg}$ system at 87.9 MeV (right). (a) Elastic scattering data and calculations obtained from semiphenomenological or Feshbach+surface potentials (full line) and Feshbach potential (dotted line); (b) imaginary potentials corresponding to Woods-Saxon (full line), Feshbach (dotted line), surface (dashed dotted line), and Feshbach+surface (dashed line); (c) radial distribution of the absorption calculated from Woods-Saxon (full line), Feshbach (dotted line), and Feshbach+surface (dashed line) potentials; (d) spin distributions deduced from Woods-Saxon or Feshbach+surface potentials (full line) and Feshbach (dotted line) potential. In upper windows the $\langle l \rangle$ and $\langle l^2 \rangle$ energy dependences calculated from Woods-Saxon potentials (triangles) are compared to the values obtained for Feshbach+surface potentials (circles) at the energies where the experiments were carried out.

A. Low lying inelastic channels contribution

In the Feshbach theory the contribution of inelastic channels to the nonlocal imaginary potential may be written as

TABLE II. Experimental charge density of ^{36}S (Ref. [19]) $\rho_c(r) = \sum_n a_n j_0(n\pi r/R)$ if $r \leq 8.0$ and $\rho_c(r) = 0$ if $r > 8.0$.

a_1	0.37032×10^{-1}	a_4	-0.19852×10^{-1}	a_7	0.37795×10^{-2}	a_{10}	0.15845×10^{-3}	a_{13}	-0.11663×10^{-4}
a_2	0.57939×10^{-1}	a_5	-0.67176×10^{-2}	a_8	-0.55272×10^{-3}	a_{11}	-0.84063×10^{-4}	a_{14}	0.35204×10^{-5}
a_3	0.10049×10^{-1}	a_6	0.61882×10^{-2}	a_9	-0.12904×10^{-3}	a_{12}	0.34101×10^{-4}	a_{15}	-0.95135×10^{-6}

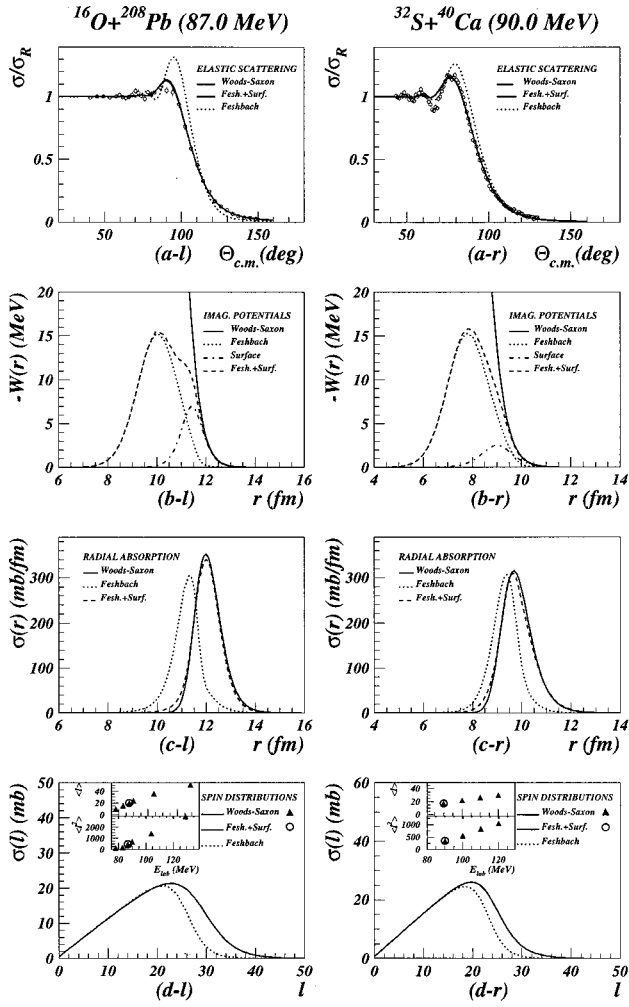


FIG. 2. Same as Fig. 1 but for the $^{16}\text{O}+^{208}\text{Pb}$ system at 87.0 MeV (left) and the $^{32}\text{S}+^{40}\text{Ca}$ system at 90.0 MeV (right).

$$\text{Im} \Delta V^{\text{in}}(\mathbf{r}, \mathbf{r}') = \sum_{i \neq 0} V_i^*(\mathbf{r}) \text{Im} G_i(\mathbf{r}, \mathbf{r}') V_i(\mathbf{r}'), \quad (2)$$

where $V_i(\mathbf{r})$ is the transition matrix element for the excitation of a state i of target or projectile and $G_i(\mathbf{r}, \mathbf{r}')$ is the Green function that describes the propagation of the system in the channel i . G_i is approximated [7] by the WKB propagator

$$G_i(\mathbf{r}, \mathbf{r}') \approx G_i^{\text{WKB}}(\mathbf{r}, \mathbf{r}') = -\frac{\mu}{2\pi\hbar^2} \frac{e^{iK_i|\mathbf{r}-\mathbf{r}'|}}{|\mathbf{r}-\mathbf{r}'|}, \quad (3)$$

where K_i is the WKB local momentum for the channel i

$$K_i^2 = \frac{2\mu}{\hbar^2} [E_{c.m.} - (E_i + U(R) + i \text{Im} \Delta V_L^{\text{in}}(R) + V_C(R))]. \quad (4)$$

$E_{c.m.}$ is the center of mass energy of the collision, E_i the excitation energy of the channel i , $U(R)$ the real potential of Eq. (1), $V_C(R)$ the Coulomb potential, and $\text{Im} \Delta V_L^{\text{in}}(R)$ the local imaginary potential coming from the inelastic channels contribution that for simplicity we write in the following $\text{Im} \Delta V_L^{\text{in}}(R) = W^{\text{in}}(R)$. K_i can be written as

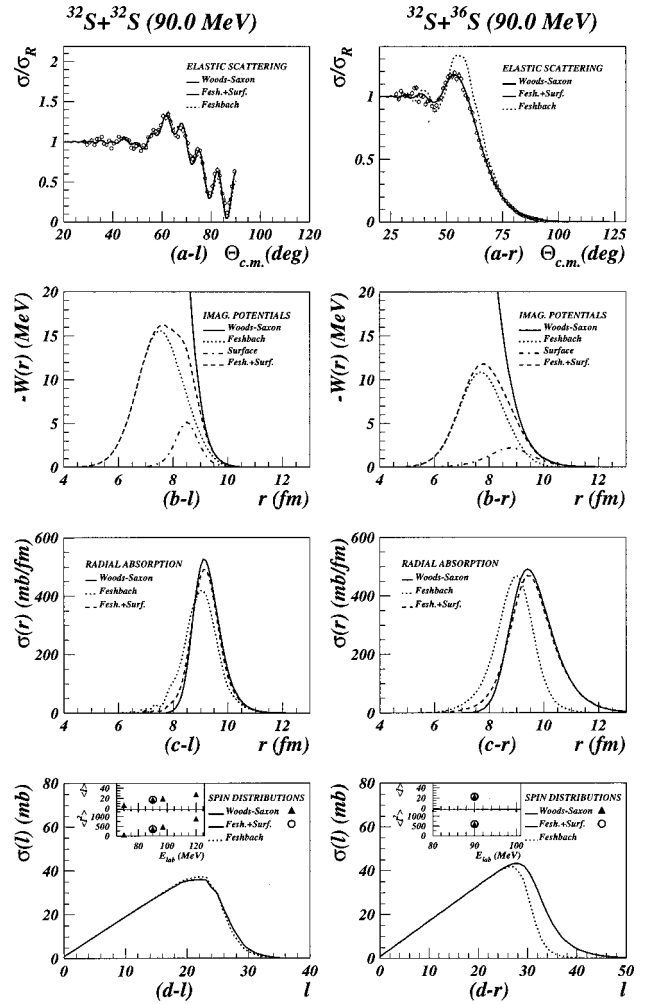


FIG. 3. Same as Fig. 1 but for the $^{32}\text{S}+^{32}\text{S}$ system at 90.0 MeV (left) and the $^{32}\text{S}+^{36}\text{S}$ system at 90.0 MeV (right).

$$K_i = k_i + i\kappa_i \quad (5)$$

with

$$k_i^2 = \frac{\mu}{\hbar^2} [E_{c.m.} - E_B^{i*}(R) + \sqrt{[E_{c.m.} - E_B^{i*}(R)]^2 + [W^{\text{in}}(R)]^2}],$$

$$\kappa_i = \frac{\mu}{\hbar^2} \frac{W^{\text{in}}(R)}{k_i}, \quad (6)$$

and

$$E_B^{i*}(R) = E_i + U(R) + V_C(R). \quad (7)$$

From Eq. (4) one can deduce that the propagator of Eq. (3) includes multistep processes. Indeed our propagator can be expanded in terms of the bare propagator, G_0 , as

$$G = G_0 + G_0 V G_0 + G_0 V G_0 V G_0 + \dots \quad (8)$$

Introducing this relation in Eq. (2), we obtain

$$\text{Im} \Delta V^{\text{in}} = \text{Im}(V G_0 V + V G_0 V G_0 V + \dots). \quad (9)$$

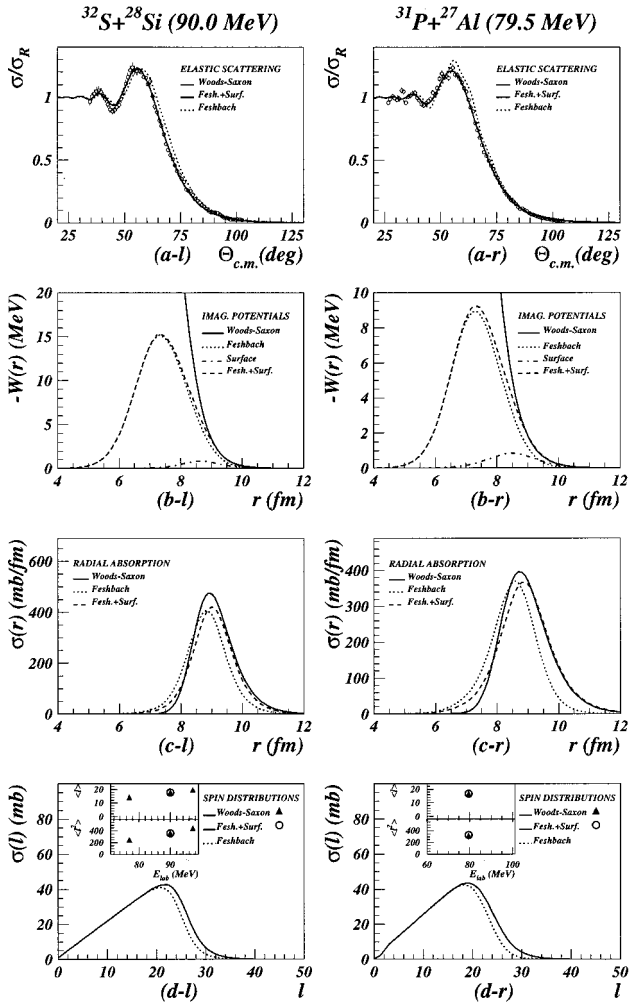


FIG. 4. Same as Fig. 1 but for the $^{32}\text{S}+^{28}\text{Si}$ system at 90.0 MeV (left) and the $^{31}\text{P}+^{27}\text{Al}$ system at 79.5 MeV (right).

The first term describes the absorption due to the direct inelastic processes while the others give the absorption corresponding to the multistep processes which take account of the compound nucleus contribution. Assuming a weak non-locality, the local nucleus-nucleus potential can be obtained as the Wigner transform of the nonlocal potential [27,28]

$$W^{\text{in}}(R) = \int e^{i\mathbf{k}\cdot\mathbf{s}} \text{Im} \Delta V^{\text{in}}(\mathbf{R}, \mathbf{s}) ds, \quad (10)$$

TABLE III. Best optical model parameters (the W_0 parameter was kept fixed).

System	E_{lab} (MeV)	N_R	W_0 (MeV)	R_W (fm)	a_W (fm)	χ^2/n	σ_R (mb)	Note
$^{31}\text{P}+^{27}\text{Al}$	79.5	1.217	60	7.378	0.471	1.80	737	
$^{35}\text{Cl}+^{24}\text{Mg}$	85.0	1.252	60	7.897	0.386	1.60	489	
$^{37}\text{Cl}+^{24}\text{Mg}$	87.9	1.366	60	7.929	0.382	0.90	508	
$^{32}\text{S}+^{28}\text{Si}$	90.0	1.410	60	7.853	0.406	1.15	749	a
$^{32}\text{S}+^{32}\text{S}$	90.0	1.672	60	8.416	0.305	2.90	631	
$^{32}\text{S}+^{36}\text{S}$	90.0	1.710	60	7.967	0.501	1.75	943	
$^{32}\text{S}+^{40}\text{Ca}$	90.0	1.419	60	8.539	0.378	3.59	473	
$^{16}\text{O}+^{208}\text{Pb}$	87.0	1.607	60	11.10	0.324	1.08	474	

^aOnly experimental data at angles $34.50^\circ \leq \theta_{\text{c.m.}} \leq 80.50^\circ$ were used in the fit. All χ^2/n values were obtained for comparison with the complete angular distributions.

where $\text{Im} \Delta V^{\text{in}}$ is the nonlocal potential of Eq. (2), now expressed in terms of \mathbf{R} and \mathbf{s} coordinates defined by

$$\mathbf{R} = \frac{\mathbf{r} + \mathbf{r}'}{2}, \quad \mathbf{s} = \mathbf{r} - \mathbf{r}'. \quad (11)$$

\mathbf{R} and \mathbf{s} are, respectively, the center of mass and relative motion coordinates and \mathbf{k} is the local momentum defined as

$$k^2 = \frac{2\mu}{\hbar^2} [E_{\text{c.m.}} - (U(R) + V_c(R))]. \quad (12)$$

In the summation over i in Eq. (2), we keep only the low lying collective states of target and projectile. Assuming vibrational states we use the collective model form factors and write

$$V_i(\mathbf{r}) = \frac{1}{\sqrt{2\lambda + 1}} f_\lambda^{(i)}(r) Y_\lambda^\mu(\mathbf{r}) \quad (13)$$

with

$$f_\lambda^{(i)}(r) = \beta_{\lambda j}^{(i)} R_j \frac{\partial U^c(r)}{\partial r}, \quad (14)$$

where $\beta_{\lambda j}^{(i)}$ is the transition amplitude of λ -multipolarity in channel i for nucleus j , R_j is the radius of the excited nucleus and $U^c(r)$ is the real nucleus-nucleus Copenhagen potential [1,29]. It was shown that the nuclear form factor of Eq. (14) reproduces the RPA-microscopic nuclear form factors at the nuclear surface [30,31]. The details of the derivation of the local potential of Eq. (10) are given in Refs. [7,10]. It gives

$$W^{\text{in}}(R) = -\frac{\mu}{2\pi k \hbar^2} \sum_{\lambda, i \neq 0} (\beta_{\lambda j}^{(i)} R_j)^2 \int_0^{2R} ds e^{-\kappa_i s} \times \sin(k s) \sin(k_i s) \frac{\partial U^c(r)}{\partial r} \Big|_{r=R+s/2} \frac{\partial U^c(r)}{\partial r} \Big|_{r=R-s/2}, \quad (15)$$

where κ_i and k_i depend upon $W^{\text{in}}(R)$. This equation is solved by iteration.

In the limit of a small nonlocality range $W^{\text{in}}(R)$ has a simple form, similar to the semiclassical polarization potential of Broglia [1,2]

TABLE IV. Low lying collective states included in Feshbach calculations.

Nucleus _{g.s.}	J^π	E_{J^π} (MeV)	$E\lambda$	β_N	Branching ratio	Mixing ratio
$^{16}\text{O}_{0^+}$	3^-	6.130	$E3$	0.71	100.0	
	2^+	6.920	$E2$	0.38	100.0	
	2^+	11.520	$E2$	0.25	100.0	
$^{24}\text{Mg}_{0^+}$	2^+	1.370	$E2$	0.60	100.0	
	2^+	4.250	$E2$	0.14	78.9	
$^{27}\text{Al}_{5/2^+}$	$3/2^+$	1.014	$E2+M1$	0.12	97.0	+0.351
	$7/2^+$	2.211	$E2+M1$	0.24	100.0	-0.468
	$9/2^+$	3.004	$E2$	0.19	88.6	
$^{28}\text{Si}_{0^+}$	2^+	1.780	$E2$	0.41	100.0	
	3^-	6.880	$E3$	0.40	100.0	
$^{31}\text{P}_{1/2^+}$	$3/2^+$	1.266	$E2+M1$	0.15	100.0	+0.300
	$5/2^+$	2.234	$E2$	0.22	100.0	
	$7/2^-$	4.431	$E3$	0.31	1.0	
$^{32}\text{S}_{0^+}$	2^+	2.230	$E2$	0.31	100.0	
	2^+	4.280	$E2$	0.12	86.0	
	3^-	5.010	$E3$	0.44	3.1	
$^{35}\text{Cl}_{3/2^+}$	$5/2^+$	1.760	$E2+M1$	0.17	100.0	+2.850
	$7/2^+$	2.650	$E2$	0.10	90.6	
	$7/2^-$	3.160	$E3$	0.10	90.0	
$^{36}\text{S}_{0^+}$	2^+	3.290	$E2$	0.16	100.0	
$^{37}\text{Cl}_{3/2^+}$	$5/2^+$	1.730	$E2+M1$	0.08	100.0	+0.250
	$5/2^+$	3.090	$E2+M1$	0.13	100.0	+1.500
	$7/2^-$	3.100	$E3+M2$	0.16	100.0	+0.180
	$9/2^-$	4.010	$E3$	0.17	31.0	
$^{40}\text{Ca}_{0^+}$	3^-	3.740	$E3$	0.40	100.0	
	2^+	3.900	$E2$	0.12	100.0	
$^{208}\text{Pb}_{0^+}$	3^-	2.600	$E3$	0.11	100.0	

$$\begin{aligned}
W^{\text{in}}(R) &= \lim_{s \rightarrow 0} \text{Im} \Delta V^{\text{in}}(R, s) \\
&= -\frac{\mu}{8\pi^2 \hbar^2} \sum_{\lambda, i \neq 0} k_i (\beta_{\lambda_j}^{(i)} R_j)^2 \left| \frac{\partial U(R)}{\partial R} \right|^2. \quad (16)
\end{aligned}$$

Our approximation to take vibrational low lying states only and to approach their form factors by a surface function implies that we have the compound states contribution at the surface only. This is an approximation but at low energy it will not affect the elastic cross sections since they are not sensitive to the potential in the interior. For higher energies our approximation would not be enough.

The imaginary potential of Eq. (15) is calculated for each system by including excited states listed for each nucleus in Table IV with their energy and vibrational amplitudes β_i . The results are displayed in Figs. 1(b) to 4(b) and compared with the phenomenological imaginary potentials of previous section. We see that except for $^{35,37}\text{Cl}+^{24}\text{Mg}$, where the phenomenological (full lines) and Feshbach (dotted lines) imaginary potentials agree for distances larger than 9.5 fm [see Fig. 1(b)], the imaginary Feshbach potential does not give enough absorption compared to phenomenology [see Figs. 2(b) to 4(b)]. As expected from our results on the imaginary potential, the inclusion of inelastic channels only is not enough to reproduce the elastic scattering cross section except for $^{35,37}\text{Cl}+^{24}\text{Mg}$. This is shown in Figs. 1(a) to 4(a)

where we compare elastic scattering calculations from phenomenological (full line) and Feshbach (dotted line) imaginary potentials.

B. Phenomenological transfer channel contribution

The lack of absorption obtained in Sec. III A with the inelastic channels only can be easily understood. Transfer cross sections have been measured for some of these systems. For $^{35,37}\text{Cl}+^{24}\text{Mg}$ the experimental transfer cross sections [10] are indeed small for the two systems. For the first system at 73.6 MeV lab, $\sigma^{\text{tr}} < 0.3$ mb and at 100.0 MeV lab, $\sigma^{\text{tr}} = 10 \pm 2$ mb, while for the second one at 76.1 MeV lab, $\sigma^{\text{tr}} < 0.6$ mb and at 103.5 MeV lab, $\sigma^{\text{tr}} = 25 \pm 3$ mb, which represent few percents of the total absorption. On the contrary, for $^{16}\text{O}+^{208}\text{Pb}$, experimental measurements performed at 86 MeV lab [32] and at 88 MeV lab [33] show that the transfer cross section represents about twenty percent of the total reaction cross section and is comparable to the inelastic cross section. In fact at 86 MeV lab, $\sigma^{\text{in}} = 87.5 \pm 26.2$ mb, $\sigma^{\text{tr}} = 81.4 \pm 10.4$ mb, $\sigma^{\text{fis-fus}} = 218 \pm 11$ mb, and $\sigma^{\text{tot}} = 384 \pm 48$ mb while at 88 MeV lab, $\sigma^{\text{in}} = 117.5 \pm 25$ mb, $\sigma^{\text{tr}} = 95.8 \pm 6.2$ mb, $\sigma^{\text{fis-fus}} = 350 \pm 40$ mb, and $\sigma^{\text{tot}} = 572 \pm 71$ mb.

These last results show that the contribution to the reaction cross section coming from the transfer processes may be very important and, consequently, we cannot reproduce in all

TABLE V. Best surface potential parameters.

System	E_{lab} (MeV)	Fesh. states (number)	σ^{in} (mb)	W_S (MeV)	R_S (fm)	a_S (fm)	χ^2/n	$\sigma^{\text{in+tr}}$ (mb)	Note b
$^{31}\text{P}+^{27}\text{Al}$	79.5	6	662	0.85	8.50	0.519	5.72	748	
$^{35}\text{Cl}+^{24}\text{Mg}$	85.0	5	484	2.14	8.44	0.280	1.58	485	
$^{37}\text{Cl}+^{24}\text{Mg}$	87.9	6	505	3.64	8.24	0.264	0.95	508	
$^{32}\text{S}+^{28}\text{Si}$	90.0	4	683	0.83	8.66	0.407	1.02	742	a
$^{32}\text{S}+^{32}\text{S}$	90.0	3	629	5.15	8.50	0.271	2.79	632	
$^{32}\text{S}+^{36}\text{S}$	90.0	4	790	2.19	8.78	0.529	2.29	942	
$^{32}\text{S}+^{40}\text{Ca}$	90.0	5	394	2.53	9.00	0.413	3.29	472	
$^{16}\text{O}+^{208}\text{Pb}$	87.0	4	373	7.00	11.43	0.294	1.00	460	

^aOnly experimental data at angles $34.50^\circ \leq \theta_{\text{c.m.}} \leq 80.50^\circ$ were used in the fit.

^bAll χ^2/n values were obtained for comparison with the complete angular distribution.

cases the elastic scattering without including the contribution coming from these processes.

Because the one-nucleon transfer cross section represents a few percent of the total measured transfer cross section [32,33], we can understand why the single-particle radial form factors of Refs. [1,2] underestimate the contribution of the transfer processes and they cannot be used to evaluate the transfer cross section. In a more consistent way, calculations assuming complicated radial form factors can be performed to evaluate the contribution to the absorptive potential coming from the multinucleon transfer processes. However this is not the aim of this paper, which is to determine the region of the potential where the absorption take place.

In order to correct this lack of absorption coming from the noninclusion of the transfer processes, we add to our imaginary potential of Eq. (15) a surface absorptive term, which simulates the contribution of these processes. We assume

$$W^{\text{tr}}(R) = -4W_s a_s \frac{df(R)}{dr} \quad (17)$$

with

$$f(r) = \frac{1}{1 + e^{(r-R_s)/a_s}}, \quad (18)$$

where W_s , R_s , and a_s are the depth, the radius and the diffusivity parameters of the potential, respectively, are fitted on elastic scattering data. In this way, the total imaginary potential is given by

$$W^{\text{tot}}(R) = W^{\text{in}}(R) + W^{\text{tr}}(R). \quad (19)$$

The $W^{\text{tr}}(R)$ term contains certainly more than transfer processes; in particular it may correct the first one, $W^{\text{in}}(R)$. This last term has been obtained by including in our Feshbach calculation all the open inelastic channels that give a contribution to the total reaction cross section higher than one percent. Consequently the corrections coming from the $W^{\text{tr}}(R)$ term must be very low and we think that this $W^{\text{tr}}(R)$ term corresponds mostly to transfer.

Table V shows, for each system, the number of inelastic channels included in the Feshbach potential calculations and the W_s , R_s , and a_s parameter values deduced from the fit of the elastic scattering data by using the total imaginary poten-

tial of Eq. (19). In this table we also include the reaction cross section σ^{in} and $\sigma^{\text{in+tr}}$ calculated with both Feshbach and Feshbach+transfer imaginary potentials. The contributions to the total reaction cross section coming from this phenomenological transfer term are compatible with the measured transfer cross sections when they are available. The contribution of $W^{\text{tr}}(R)$ (dotted-dashed lines) as well as the total imaginary potential (dashed lines) are drawn in Figs. 1(b) to 4(b). One can observe that there exists a large radial domain in which both Woods-Saxon and total imaginary potential of Eq. (19) are in good agreement. The contribution of $W^{\text{tr}}(R)$ is weak for the $^{35,37}\text{Cl}+^{24}\text{Mg}$ systems for which the transfer cross section is weak, while it is important for the other analyzed systems. For these ones the inclusion of this transfer term is crucial. In Figs. 1(a) to 4(a) we only show the calculation with the imaginary potential of Sec. II because it is not possible to distinguish between elastic scattering cross sections calculated with both imaginary potentials of Sec. II and Eq. (19).

IV. RADIAL AND SPIN DISTRIBUTIONS OF REACTION CROSS SECTION

The total reaction cross section, σ_R , can be written as [34]

$$\sigma_R = -\frac{1}{(2I_P+1)(2I_T+1)} \frac{2}{\hbar v_0} \langle \chi_0^+ | W^{\text{tot}}(r) | \chi_0^+ \rangle, \quad (20)$$

where I_P and I_T are the intrinsic spin of the projectile (I_P) and target (I_T) nuclei in their ground states while v_0 and χ_0^+ are the velocity and wave function of the relative motion in the elastic channel at the energy $E_{\text{c.m.}}$. Introducing the partial wave expansion of χ_0^+

$$\chi_0^+ = \frac{1}{kr} \sum_l i^l (2l+1) \chi_l(r) P_l(\cos \theta) \quad (21)$$

in Eq. (20), one can write

$$\sigma_R = \int_0^\infty \sigma(r) dr \quad (22)$$

with

TABLE VI. Total reaction cross section and angular momentum mean values.

System	E_{lab} (MeV)	Semiphenom. calculations				Fesh.+phen. surf. calculations			
		$\langle l \rangle$	$\langle l^2 \rangle$	σ_R (mb)	χ^2/n	$\langle l \rangle$	$\langle l^2 \rangle$	$\sigma^{\text{in+tr}}$ (mb)	χ^2/n
$^{31}\text{P}+^{27}\text{Al}$	79.5	16.57	318.12	737	1.80	16.70	323.20	748	5.72
$^{35}\text{Cl}+^{24}\text{Mg}$	85.0	13.13	202.32	489	1.60	13.00	197.41	485	1.58
$^{37}\text{Cl}+^{24}\text{Mg}$	87.9	13.45	211.41	508	0.90	13.39	209.88	508	0.95
$^{32}\text{S}+^{28}\text{Si}$	90.0	17.78	364.35	749	1.15	17.69	359.99	742	1.02 a
$^{32}\text{S}+^{32}\text{S}$	90.0	17.51	352.68	631	2.90	17.47	350.71	632	2.79
$^{32}\text{S}+^{36}\text{S}$	90.0	22.76	597.03	943	1.75	22.77	597.72	942	2.29
$^{32}\text{S}+^{40}\text{Ca}$	90.0	17.23	347.16	473	3.59	17.24	348.00	472	3.29
$^{16}\text{O}+^{208}\text{Pb}$	87.0	20.15	475.00	474	1.08	19.95	464.38	460	1.00

^aOnly experimental data at angles $34.50^\circ \leq \theta_{\text{c.m.}} \leq 80.50^\circ$ were used in the fit. All χ^2/n values were obtained for comparison with the complete angular distributions.

$$\sigma(r) = -\frac{1}{(2I_P+1)(2I_T+1)} \times \sum_T \frac{8\pi}{k^2 \hbar v_0} (2l+1) |\chi_l(r)|^2 W^{\text{tot}}(r), \quad (23)$$

where k is the wave number.

The ECIS94 code [26] was used to calculate the $\chi_l(r)$ wave functions with the different imaginary potentials described in Sec. II, Sec. III A, and Sec. III B. The corresponding $\sigma(r)$ functions are drawn in Figs. 1(c) to 4(c). These curves describe the radial distribution of the cross section reaction. Because we assume in all calculations the same real potential, our calculations give a direct comparison between the absorptive part of the potentials. Figures 1(c) to 4(c) show the radial distributions of the reaction cross section calculated with (1) the imaginary Woods-Saxon potentials (full lines) of Table III, (2) the microscopic Feshbach imaginary potentials (dotted lines) that include the states shown in Table IV, and (3) the imaginary potentials coming from the contribution of the Feshbach potential plus our phenomenological surface term of Table V. We see [Figs. 1(c) to 4(c)] that absorption takes place at large distances only where Woods-Saxon and $W^{\text{tot}}(r)$ imaginary potentials are in good agreement [Figs. 1(b) to 4(b)]. It shows explicitly why one can reproduce with a similar quality the experiments at energies close to the barrier, either by using a Woods-Saxon or a surface imaginary potential including inelastic and transfer processes only.

From Eqs. (20) to (23) the total reaction cross section, σ_R , can be rewritten as

$$\sigma_R = \sum_l \sigma_R(l) \quad (24)$$

with

$$\sigma_R(l) = -\frac{1}{(2I_P+1)(2I_T+1)} \frac{8\pi}{k^2 \hbar v_0} (2l+1) \times \int_0^\infty |\chi_l(r)|^2 W^{\text{tot}}(r) dr, \quad (25)$$

where the function $\sigma_R(l)$ gives the contribution of each partial wave to the total absorption. In Figs. 1(d) to 4(d) the spin distributions as well as the $\langle l \rangle$ and $\langle l^2 \rangle$ values calculated with the potentials of Table III (full lines and filled triangles in upper windows, respectively) are compared with those calculated at one energy with the $W^{\text{tot}}(r)$ potential of Eq. (19) (full lines and open circles). In the upper windows we have included the $\langle l \rangle$ and $\langle l^2 \rangle$ values taken from Ref. [35] where they have been calculated at different energies in the same way described in Sec. II. Calculations with potentials of Sec. II and Eq. (19) are indistinguishable. Comparison with calculations performed with Feshbach potentials only (dotted lines) allows to show the importance of transfer processes. In Table VI the $\langle l \rangle$, $\langle l^2 \rangle$, and σ_R values calculated from potentials of Table III and Eq. (19) are compared. The χ^2/N values obtained in the fit of the elastic scattering data with the two above mentioned potentials are also given.

V. CONCLUSIONS

Elastic scattering angular distributions for different systems, at energies close to the Coulomb barrier, have been analyzed in a systematic way. First the data have been fitted by using a renormalized M3Y double folding real potential and a fitted Woods-Saxon imaginary potential. These standard calculations have been taken as a reference for all the other calculations performed in this paper. Then an attempt to analyze the absorption in terms of couplings of the elastic channel to nonelastic channels has been proposed. In the Feshbach formalism the contribution of low lying inelastic channels has been first evaluated. These couplings are too weak to reproduce the data in all systems except the strongly deformed $^{35,37}\text{Cl}+^{24}\text{Mg}$. This lack of absorption is assumed to come from transfer channel couplings what is supported by the measured transfer cross sections. Such transfer channels are known to give a long range surface contribution and they have been introduced empirically as a parametrized surface term added to the inelastic channels contributions. The data are now very well reproduced. The added absorptive term has a larger radius than inelastic couplings accordingly to what one expects from transfer contributions [2]. The increment on the total reaction cross section due to this long range term has been calculated and is close to the measured

transfer cross sections when they are available what shows that this empirical surface term comes mainly from transfer couplings.

The radial distribution of the reaction cross reaction has been calculated. It is concentrated in the far surface of the absorptive potential. At low energy only the tail of the imaginary potential contributes to the reaction cross section which means that good fits to data can be obtained with either a Woods-Saxon or a surface imaginary total potential and that

the volume absorption gives an inefficient contribution to the reaction cross section.

ACKNOWLEDGMENTS

The authors wish to express their gratitude to N. Vinh Mau for her constant interest and for stimulating discussions. This work has been partially supported by CICYT under the project AEN96-1662.

-
- [1] R. A. Broglia, G. Pollarolo, and A. Winther, *Nucl. Phys.* **A361**, 307 (1981).
- [2] G. Pollarolo, R. A. Broglia, and A. Winther, *Nucl. Phys.* **A406**, 369 (1983).
- [3] H. Feshbach, *Ann. Phys. (N.Y.)* **5**, 357 (1958); **19**, 287 (1962).
- [4] M. A. Andrés, F. Catara, and F. G. Lanza, *Inst. Phys. Conf. Ser.* **110**, 231 (1990); *Phys. Rev. C* **44**, 2709 (1991).
- [5] W. G. Love, T. Terasawa, and G. R. Satchler, *Nucl. Phys.* **A291**, 183 (1977); Z. El-Itaoui, P. J. Ellis, and B. A. Mugh-rabe, *ibid.* **A441**, 511 (1985); K. I. Kubo, *ibid.* **A534**, 381 (1991).
- [6] K. I. Kubo and R. E. Hodgson, *Nucl. Phys.* **A366**, 310 (1981).
- [7] N. Vinh Mau, *Nucl. Phys.* **A457**, 413 (1986); **A470**, 406 (1987); *Inst. Phys. Conf. Ser.* **110**, 1 (1990).
- [8] J. L. Ferrero, J. C. Pacheco, A. Baeza, J. M. Barrigón, B. Bilwes, R. Bilwes, and N. Vinh Mau, *Nucl. Phys.* **A514**, 367 (1990); B. Bilwes, R. Bilwes, N. Vinh Mau, J. L. Ferrero, and J. C. Pacheco, *ibid.* **A526**, 292 (1991); N. Vinh Mau, J. L. Ferrero, J. C. Pacheco, and B. Bilwes, *ibid.* **A531**, 435 (1991); *Phys. Rev. C* **47**, 899 (1993).
- [9] N. Vinh Mau, J. C. Pacheco, J. L. Ferrero, and B. Bilwes, *Nucl. Phys.* **A560**, 879 (1993).
- [10] J. M. Barrigón, A. Baeza, J. L. Ferrero, J. C. Pacheco, B. Bilwes, and R. Bilwes, *Nucl. Phys.* **A545**, 720 (1992); J. M. Barrigón, Doctoral thesis, Universidad de Extremadura, Spain, 1991.
- [11] J. C. Pacheco, B. Bilwes, F. Sánchez, J. A. Ruíz, J. Díaz, J. L. Ferrero, and D. Kadi-Hanifi, *Nucl. Phys.* **A588**, 537 (1995).
- [12] B. Bilwes, R. Bilwes, F. Ballester, J. Díaz, J. L. Ferrero, C. Roldán, L. Stuttgé, and F. Sánchez, *Nucl. Phys.* **A473**, 353 (1987).
- [13] J. L. Ferrero, J. A. Ruíz, B. Bilwes, and R. Bilwes, *Nucl. Phys.* **A510**, 360 (1990).
- [14] B. Bilwes, R. Bilwes, J. L. Ferrero, D. Pocanic, and L. Stuttgé, *Nucl. Phys.* **A463**, 731 (1987).
- [15] A. Baeza, B. Bilwes, R. Bilwes, J. Díaz, and J. L. Ferrero, *Nucl. Phys.* **A419**, 412 (1984); J. Díaz, J. L. Ferrero, J. A. Ruíz, B. Bilwes, and R. Bilwes, *ibid.* **A494**, 311 (1989).
- [16] R. Vandenbosch and M. P. Webb, University of Washington Nuclear Physics Laboratory Annual Report, 1975 (unpublished), p. 136.
- [17] G. R. Satchler and W. G. Love, *Phys. Rep.* **55**, 183 (1979).
- [18] G. Bertsch, J. Borysowicz, H. McManus, and W. G. Love, *Nucl. Phys.* **A284**, 399 (1977).
- [19] H. de Vries, C. W. de Jager, and C. de Vries, *At. Data Nucl. Data Tables* **36**, 495 (1987).
- [20] D. M. Brink and N. Takigawa, *Nucl. Phys.* **A279**, 159 (1977).
- [21] G. C. Li and M. R. Yerman, *Phys. Rev. C* **9**, 1861 (1974).
- [22] W. J. Briscoe, H. Crannell, and J. C. Bergstrom, *Nucl. Phys.* **A344**, 475 (1980).
- [23] R. F. Frosch, R. Hofstadter, J. S. Mc Carthy, G. K. Noldeke, K. J. Van Oostrum, B. C. Clark, R. Herman, and D. G. Ravenhall, *Phys. Rev.* **174**, 1380 (1968).
- [24] M. Brack, C. Guet, and R. B. Hakansson, *Phys. Rep.* **123**, 274 (1985).
- [25] R. D. Woods and D. S. Saxon, *Phys. Rev.* **95**, 577 (1954).
- [26] J. Raynal, Nuclear Data Bank of the OCDE (1994).
- [27] F. G. Perey and B. Buck, *Nucl. Phys.* **32**, 363 (1962); R. Peierls and N. Vinh Mau, *Nucl. Phys.* **A343**, 1 (1980).
- [28] F. G. Perey and D. S. Saxon, *Phys. Lett.* **10**, 107 (1964); H. Horinchi, *Prog. Theor. Phys.* **64**, 184 (1980).
- [29] R. A. Broglia and A. Winther, *Heavy Ion Reactions* (Benjamin/Cumming, Reading, MA, 1981), Sec. III.1, p.114.
- [30] R. A. Broglia and A. Winther, *Heavy Ion Reactions* (Ref. [29]), Sec. IV.3.
- [31] R. A. Broglia, C. H. Dasso, G. Pollarolo, and A. Winther, *Phys. Rep.* **48**, 351 (1978).
- [32] J. Lilley (private communication).
- [33] F. Videbaek, R. B. Golgstein, L. Grodzins, S. G. Steadman, T. A. Belote, and J. D. Garrett, *Phys. Rev. C* **15**, 954 (1977).
- [34] G. R. Satchler, *Direct Nuclear Reactions* (Oxford University Press, New York, 1983), Sec. 4.3, p. 126.
- [35] M. D. Kadi-Hanifi, thèse d'état, Université d'Alger, Algeria, 1999.